nature photonics

SUPPLEMENTARY INFORMATION
https://doi.org/10.1038/s41566-017-0070-7

In the format provided by the authors and unedited.

Tandem luminescent solar concentrators based on engineered quantum dots

Kaifeng Wu[1,2], Hongbo Li[1,3] and Victor I. Klimov[1*]

[1]Centre for Advanced Solar Photophysics, Los Alamos National Laboratory, Los Alamos, NM, USA. Present addresses: [2]State Key Laboratory of Molecular Reaction Dynamics and Collaborative Innovation Center of Chemistry for Energy Materials, Dalian Institute of Chemical Physics, Chinese Academy of Sciences, Dalian, China. [3]School of Materials Science and Engineering, Beijing Institute of Technology, Beijing, China. Kaifeng Wu and Hongbo Li contributed equally to this work. *e-mail: klimov@lanl.gov

Supplementary Information for

Tandem luminescent solar concentrators based on engineered quantum dots

Kaifeng Wu[1,2], Hongbo Li[1,3], and Victor I. Klimov[1]*

[1]Centre for Advanced Solar Photophysics, Los Alamos National Laboratory, Los Alamos, New Mexico 87545, USA

[2]Present address: State Key Laboratory of Molecular Reaction Dynamics and Collaborative Innovation Center of Chemistry for Energy Materials, Dalian Institute of Chemical Physics, Chinese Academy of Sciences, 457 Zhongshan Road, Dalian 116023, China.

[3]Present address: School of Materials Science and Engineering, Beijing Institute of Technology, Beijing, China

* Address correspondence to klimov@lanl.gov

This file includes:

Supplementary Note 1. Modelling of optical quantum efficiencies of planar LSCs

We adopt the analytic model developed in ref. 1 for calculating the optical quantum efficiencies (external and internal) of planar LSCs. The optical scattering in the LSC waveguide was not considered in the original model [1]. Here we include the scattering effects by introducing the scattering coefficient s_2 for light re-emitted by LSC fluorophores. In this model, the internal quantum efficiency (IQE; η_{int}) or the collection efficiency (η_{col}) is treated as the sum of the collection efficiencies for different-generation photons. Following the procedure of ref. 1, we obtain:

$$\eta_{int} = \eta_{col} = \frac{\eta_{PL}\eta_{trap}}{1+\beta(\alpha_2+s_2)L\left[1-\left(\frac{\alpha_2\eta_{PL}+s_2}{\alpha_2+s_2}\right)\eta_{trap}\right]}, \qquad \text{(S1)}$$

where α_2 is the absorption coefficient of the LSC fluorophores at the emission wavelength, β is a constant (~1.4), L is the LSC length, η_{PL} is the PL QY of QDs measured in dilute solutions, and η_{trap} is the efficiency of light trapping into waveguide modes (75% for a waveguide with the refractive index n =1.5). If scattering is ignored, eq. S1 reduces to

$$\eta_{int} = \eta_{col} = \frac{\eta_{PL}\eta_{trap}}{1+\beta\alpha_2 L\left(1-\eta_{PL}\eta_{trap}\right)}, \qquad \text{(S2)}$$

which is the same as the expression obtained in the original model of ref. 1.

In the case of zero reabsorption (α_2 = 0), scattering becomes the efficiency-limiting factor. This situation is realized in our Mn^{2+}-doped QD LSCs, where we have

$$\eta_{int} = \eta_{col} = \frac{\eta_{PL}\eta_{trap}}{1+\beta s_2 L\left(1-\eta_{trap}\right)} \;. \qquad \text{(S3)}$$

Note that all the previous derivations have been performed for single-wavelength absorption or scattering coefficients α_2 and s_2, which is a good approximation when the PL is narrow. If the PL band is broad, the situation we encounter with the $CuInSe_2$ QDs, the collection efficiency can be obtained by spectrally average eqs. S1-S3 over the PL band, $\Phi_{PL}(\nu)$, of the QDs. For instance, the averaged eq. S2 becomes:

$$\eta_{int} = \frac{\int \eta_{PL}\eta_{trap}\left[1+\beta\alpha(\nu)L\left(1-\eta_{PL}\eta_{trap}\right)\right]^{-1}\Phi_{PL}(\nu)\,d\nu}{\int \Phi_{PL}(\nu)\,d\nu}. \tag{S4}$$

Another point worth noting is that for our layered LSCs where a thin QD/polymer layer (thickness d) is deposited onto a much thicker glass substrate (thickness D), α_2 is an effective absorption coefficient determined from $\alpha_{2,\mathrm{eff}} = \alpha_2 d/(D + d)$; see ref. 2.

Supplementary Note 2. Derivation of internal quantum efficiencies of LSCs from electro-optical measurements

A detailed derivation of the relationship between the power conversion efficiencies (PCE) of a standalone photovoltaic (PV) cell (η_{PV}) and a coupled LSC-PV system ($\eta_{\mathrm{LSC\text{-}PV}}$) was done in our previous work[2]. According to these calculations,

$$\eta_{LSC-PV} = \frac{\langle Q_{PL}\rangle}{\langle Q_s\rangle}\eta_{s,abs}\eta_{int}\eta_{PV} = q\eta_{s,abs}\eta_{int}\eta_{PV}, \tag{S5}$$

where q is the "spectral re-shaping" factor of the LSC defined as $q = \langle Q_{PL}\rangle / \langle Q_s\rangle$, and $\langle Q_s\rangle$ and $\langle Q_{PL}\rangle$ are the external quantum efficiencies (Q) of the PV device averaged over the solar spectrum and the LSC PL spectrum, respectively. The IQE (η_{int}) of the LSC can be obtained by comparing the short-circuit current densities (J_{sc}) of the LSC-PV system and the standalone PV:

$$\eta_{int} = \frac{J_{sc,LSC-PV}}{q\eta_{s,abs}J_{sc}G} \quad . \tag{S6}$$

Supplementary Note 3. Calculations of visible transmittance

The weighted average visible transmittance (*VT*) of an LSC window can be calculated from:[3]

$$VT = \frac{\int T(\lambda)P(\lambda)S(\lambda)d\lambda}{\int P(\lambda)S(\lambda)d\lambda} \quad , \tag{S7}$$

where λ is the light wavelength, $T(\lambda)$ is the transmittance of the window, $P(\lambda)$ is the photopic response function of a typical human eye, and $S(\lambda)$ is the solar spectrum. $T(\lambda)$ of a QD-LSC is given by $T(\lambda)=(1-R)10^{-OD(\lambda)}$, where R is the reflectance of a glass window and $OD(\lambda)$ is the optical density of the QD layer. For CISe-QD LSCs, the absorption of QDs in the visible range is strong so that only reflectance from the front glass surface is considered; hence, $R \approx 4\%$. For Mn-QD LSCs, the QDs have very weak absorption in the visible range so that the reflectances from both the front and back glass surfaces have to be considered; hence, $R \approx 8\%$. Using $OD(\lambda)$ spectra of QD samples, we calculate *VT* for CISe-QD and Mn^{2+}-doped QD LSCs with different QD concentrations. The results of these calculations are shown in Fig. 2c and Supplementary Fig. 11, respectively.

According to ref. 4, clear (untinted) architectural window glass typically has a *VT* of 82-90%. Therefore, for all concentrations of Mn^{2+}-doped QDs considered in Supplementary Fig. 11 ($\eta_{s,abs}$ within 6%), the QD-LSCs can be qualified as clear architectural windows. Tinted architectural window glass has a lower *VT* in the range of 40-62%.[4] CISe QD-LSCs with $\eta_{s,abs}$ <20% (Fig. 2c) meet this requirement (*VT*>44%) and, therefore, can function as tinted architectural windows.

Supplementary Note 4. Comparison to literature devices

It is instructive to compare the performance of our devices to those of the highest-efficiency LSCs based on QDs[2,5-11] and dye molecules[12-14] reported in the literature (see Supplementary Fig. 13 and Supplementary Tables 1 and 2). As figures of merit for this comparison, we use the optical power efficiency ($\eta_{s,p}$) under sunlight illumination (see our earlier discussion) and, when available, the PCE of coupled LSC-PV devices.

Based on $\eta_{s,p}$, our single-layer CISe QD-LSCs are superior to any of the reported QD-LSCs for all size regimes, and the performance gap further increases for tandem devices (see Supplementary Fig. 13). For example, record-performing LSCs based on $CuInSe_{2-x}S_x$ QDs[9] and Si QDs[10] exhibited $\eta_{s,p}$ of 3.2% and 2.85%, respectively, for the 144 cm^2 device area. On the other hand, our single-layer CISe QD-LSCs of a much larger area of 230 cm^2 show $\eta_{s,p}$ of 5.5%, which is further boosted to 7.8% in the case of the tandem structures.

Dye-based LSCs have been studied for decades, and therefore, are in general better developed than QD-LSCs. There are several literature demonstrations of PCEs of up to 5 - 7% for coupled LSC-PV devices. [12-15] These demonstrations, however, employ fairly small-area structures (≤25 cm^2) aided by back reflectors (see Supplementary Table 2). For example, record-performing LSCs based on a two-dye mixture of ref. 13 showed PCEs of 7.1% and 5.3% with and without a diffusive back reflector, respectively. These efficiencies were observed for a 25-cm^2 device area, which is considerably smaller than that of our devices. Applying a typical dependence of η_{int} on LSC size[1], we can use the above values to project the performance of these devices for larger dimensions. Based on these projections (see Supplementary Figure 13), we obtain that even in the most favourable scenario of negligible losses to scattering, the PCEs of the above structures would drop to approximately 2.3% and 1.7% for the 230 cm^2 device area for the situations with and without a back reflector, respectively. Even the larger of these values is considerably lower (by ~30%) than the PCE of our QD tandem (3.1%) obtained in a semitransparent device not supplemented by the back reflector.

The above comparison of our present results to available literature examples of record-performing LSCs indicates a considerable promise of QD-based structures and especially QD tandems for the realization of devices that can maintain strong performance even for large slab areas required for the practical implementation of the LSC technology.

Supplementary Table 1. Overview of literature results for QD-based LSCs [1)]

Ordered by LSC area	QD Type	QD QY	LSC Size (L× W × T) cm×cm×cm	Optical Power Efficiency [2)]	Power Conversion Efficiency	Notes
Small, 2016, 12,	CdSe/Cd$_x$Pb$_{1-x}$S core/alloyed	40%	7 × 1.5 × 0.3	1.4%	1.15%	3)

5354-5365. Ref. 5	shell					
Adv. Energy Mat., 2016, 6, 1501913. Ref. 6	PbS/CdS core/shell	40-50%	10 × 1.5 × 0.2	1.0%	NA	4)
Nat. Photon, 2014, 8, 392-399. Ref. 7	CdSe/CdS core/shell	45%	21.5 × 1.35 × 0.5	0.60%	NA	5)
J. Phys. Chem. C, 2017, 121, 3252-3260. Ref. 8	$CuInS_2$/CdS core/shell	75%	7.5×7.5 × 0.28	5.7%	NA	
Nat. Energy,	Silica-coated CdSe/Cd_{1-x}	70%	10.2 × 10.2 × 0.16	1.9%	NA	

2016, 1, 16157. Ref. 2	Zn_xS core/alloyed shell					
Nat. Nanotech., 2015, 10, 878-885. Ref. 9	$CuInSe_xS_{2-x}/ZnS$ core/shell	40%	12 × 12 × 0.3	3.2%	NA	
Nat Photon., 2017, 11, 177-185. Ref. 10	Si	50%	12 × 12 × 0.26	2.85%	NA	
Present study	$CuInSe_2/ZnS$	72%	15.2 × 15.2 × 0.16	5.5%	2.5%	
Present study	$CuInSe_2/ZnS$ +$Mn:Cd_xZn_{1-x}S$ /ZnS	72% +79%	15.2 × 15.2 × 0.16	7.8%	3.1%	

1) Only the LSCs measured under sunlight illumination (natural or simulated) are listed. Devices measured under single-wavelength excitation are not included due to difficulties in obtaining accurate values of $\eta_{s,ext}$ based on single-wavelength results.

2) The relation between the external optical power efficiency and the external quantum efficiency can be found in the main text.

3) Three edges and the bottom of the LSC slab were terminated with mirrors.

4) Three edges of the LSC slab were terminated with mirrors.

5) White diffuse reflectors were placed in the proximity of the long-face edges of the LSC.

Supplementary Table 2. Overview of literature results for dye-molecule-based LSCs

Ordered by LSC area	Lumophore Type	Lumophore QY	LSC Size (L×W×T) cm×cm×cm	Power Conversion Efficiency	Notes
Sol. Energ. Mat. Sol. Cells 2009, 93, 176-182. Ref. 12	BA241 + BA856 tandem	NA	2 × 2 × 0.3	6.7%	1)
Adv. Opt. Mater. 2014, 2, 606-611. Ref. 16	CY	~20%	2 × 2 × 0.1	0.4%	
Adv. Energy Mater. 2013, 3, 1143-1148. Ref. 17	$(TBA)_2MoCl_4$	~70%	2.5× 2.5 × 0.1	0.44%	

Science 2008, 321, 226-228. Ref. 14	DCJTB + Pt(TPBP) tandem	~70% + 50%	2.5× 2.5 × 0.2	6.8%	2), 3)
Phys. Status Solidi Rapid Res. Lett. 2008, 2, 257-259. Ref. 13	Lumogen F Red305 + Fluorescence Yellow CRS040 mixed	NA	5×5 × 0.5	7.1% or 5.3%	4)
Present study	$Mn:Cd_xZn_{1-x}S/ZnS$ + $CuInSe_2/ZnS$ tandem	79% + 72%	15.2 × 15.2 × 0.16	3.1%	

1) A white reflector was placed at the bottom of the LSC plate.

2) A mirror was placed at the bottom of the LSC plate.

3) This value is not a directly-measured result; the measurements were performed using a single-wavelength, point-by-point excitation and the obtained efficiencies were used to calculate the power conversion efficiency under sunlight illumination.

4) The PCE was 7.1% when a white reflector was placed at the bottom of the LSC plate; the PCE was 5.3% when the reflector was absent.

Supplementary Note 5. Comparing costs of solar electricity between a standalone PV and a coupled LSC-PV system

Equation S5 for PCE corresponds to the situation of a fixed power of incident solar light. Under realistic outdoor conditions, however, the incident power changes during the day due, *e.g.*, to changes in the incident angle (θ) and relative amounts of direct versus diffuse light. It turns out the dependence of PCE on θ is considerably weaker in the case of a LSC-PV system compared to a standalone PV (Supplementary Fig. 16). As a result, the angle-averaged PCE of the LSC-PV ($\langle \eta_{LSC-PV} \rangle$) is greater than that of the PV ($\langle \eta_{PV} \rangle$), which can be accounted for by an angular correction factor (χ_θ). This leads to the following modified form of eq. S5 for angle-averaged PCEs:

$$\langle \eta_{LSC-PV} \rangle = \chi_\theta q \eta_{s,abs} \eta_{int} \langle \eta_{PV} \rangle . \tag{S8}$$

Based on the data of Supplementary Fig. 16, χ_θ is ~1.4.

Next, we use eq. S8 to calculate the LSC cost-efficiency factor defined as the ratio of the per-W costs of solar electricity for the LSC-PV and PV-only systems (r_{LSC-PV}) following the formalism of ref. 2. This yields the following expression:

$$r_{LSC-PV} = \frac{f + G^{-1}}{\chi_\theta q \eta_{s,abs} \eta_{\text{int}}} \quad . \tag{S9}$$

where χ_θ is ~1.4, q is ~0.95 when pairing our LSCs with commercial Si PVs , and f is the ratio of the per-m^2 costs of the LSC and the PV module evaluated below.

The total per-m^2 cost of a QD-LSC is comprised of the costs of QDs, polymer (PVP in our case), and a glass substrate. To estimate the cost of the QDs, we consider the situations of both research-lab-scale production and large-scale industrial production. In the first scenario, the cost of chemicals is estimated based on the Sigma Aldrich catalogue (Supplementary Table 3), while in the second scenario, the prices are based on quotations from on-line retailers such as Alibaba and LookChem (Supplementary Table 4). To make our estimations more up-to-date, we have considered only online suppliers that show actual transactions within the past six months. Supplementary Tables 5 and 6 provide cost estimations for $CuInSe_2/ZnS$ and Mn^{2+}-doped $Cd_xZn_{1-x}S/ZnS$ QDs, respectively, calculated using prices of chemicals from Supplementary Tables 3 and 4. The QD amounts correspond to those produced in a single synthetic procedure described in Materials and Methods.

In addition to the costs of the materials, in our estimations have also accounted for other expenditures such as labour, usage of equipment, *etc*. To estimate non-material-related costs, we use guidelines from the silicon PV industry. According to http://pv.energytrend.com/pricequotes.html, the current price of polycrystalline silicon is ~$16/kg. Considering the low-cost of raw materials, we attribute this per-kg cost entirely to non-material-related expenses. Accordingly, we include this amount ($0.016/g) in our price estimations as an additional expense in the QD production. Based on all of these considerations, the total costs of mass-produced $CuInSe_2/ZnS$ and Mn^{2+}-doped $Cd_xZn_{1-x}S/ZnS$ QDs are ~$0.59/g and ~$0.34/g, respectively.

Fabrication of a 1×1 m^2 CISe-QD LSC with the solar absorptance $\eta_{s,abs}$ = 24% (same as in the bottom-layer LSC of the tandem in the main text) requires 1.95 g of QDs and 60 g of PVP. Considering the PVP cost of ~$0.004/g (Alibaba, https://www.alibaba.com/product-detail/Pvp-k30-polyvinylpyrrolidone-pvp-k30-price_60335761992.html?spm=a2700.7724838.0.0.0CZETH) and using the QD cost in the case of mass production, we obtain that the total cost of the CISe QD/polymer coating is $1.39/$m^2$. To fabricate a 1×1 m^2 LSC based on Mn-doped II-VI QDs used in the tandem LSC ($\eta_{s,abs}$ = 4.6%), one will need 1.13 g of the QDs and 60 g of PVP, leading to a total cost of $0.62/$m^2$ for the Mn-doped QD/polymer coating. An additional expense is associated with the cost of glass substrates. In our estimations, we assume that each type of the QD/polymer coatings is deposited onto a high-quality borosilicate glass substrate, with the two LSCs in the tandem naturally forming a self-protected, double-layered structure. According to the Alibaba price list, the cost of high-optical-quality borosilicate glass, which is similar to that used in the present study, is ~$1/$m^2$ (https://www.alibaba.com/product-detail/High-Quality-2mm-Tempered-Borosilicate-Glass_60592663557.html?spm=a2700.7724838.0.0.uF1T6a). This leads to the total cost of glass materials of $2/$m^2$ for a 1x1 m^2 tandem LSC. Approximating the cost of other constituents required to assemble a complete device by $1/$m^2$ (ref. 2), the total cost of the tandem LSC is ~$5.01/$m^2$ (Supplementary Table 7). This is approximately 20 times lower than the typical cost of the Si-PV module (~$100/$m^2$, ref. 18) yielding *f* of ~0.05 (see eq. S9). The cost of QD-LSCs with other values of $\eta_{s,abs}$ can be calculated in a similar way by adjusting the amount of the QDs used in a specific device.

In Fig. 4c (main text), we show the calculations of $r_{\text{LSC-PV}}$ conducted as a function of absorptance of the bottom layer and the LSC length for the fixed absorptance of the top layer of 4.6% which is the same as in the tested device (Fig. 4a,b). Based on these calculations, using the developed tandems one can, in principle, achieve ~28% saving in the cost of solar electricity *versus* a standalone PV module. As illustrated in Fig. 4d, a further reduction in $r_{\text{LSC-PV}}$ is possible by increasing the absorptance of the top layer to the saturated value of 6.0% (Fig. 4d), which yields $r_{\text{LSC/PV}}$ =0.66 and the corresponding cost saving of 34%.

In addition to serving as a supplement to traditional PV panels, LSCs can enable novel energy conversion devices such as solar windows. In this case, the cost of glass substrates can be excluded from the cost estimations as QD/polymer composites are directly integrated into the existing building windows. In this scenario, the per-m^2 LSC cost for our tandems drops to just \$3.01/m^2, indicating f of ~0.03. The calculations of the LSC cost-efficiency factor (Supplementary Fig. 17) suggest that in this case, the cost saving can be as high as 51% with the absorptance of the top layer of 4.6% (Supplementary Fig. 17a); it can be slightly increased (to 52%) by increasing the top-layer absorptance to 6.0% (Supplementary Fig. 17b).

Supplementary Table 3. Cost of chemicals for lab-scale production

Chemical	Batch size	Price per batch ($)	Price per g or mL	Source link
CuI	1000 g	375.5	$0.38/g	http://www.sigmaaldrich.com/catalog/product/sial/03140?lang=en&region=US
$In(Ac)_3$	50 g	390	$7.8/g	http://www.sigmaaldrich.com/catalog/product/aldrich/510270?lang=en&region=US
$Zn(St)_2$	3000 g	109	$0.036/g	http://www.sigmaaldrich.com/catalog/product/aldrich/307564?lang=en&region=US
Se	250 g	125.5	$0.50/g	http://www.sigmaaldrich.com/catalog/product/aldrich/209651?lang=en&region=US
OA	4000 mL	122	$0.030/mL	http://www.sigmaaldrich.com/catalog/product/aldrich/364525?lang=en&region=US
OAm	1845 mL	264	$0.14 /mL	http://www.sigmaaldrich.com/catalog/product/aldrich/htoa100?lang=en&region=US
DPP	2625 mL	2625	$2.8/mL	http://www.sigmaaldrich.com/catalog/product/aldrich/252964?lang=en&region=

				US
DDT	18000 mL	442	$0.024/mL	http://www.sigmaaldrich.com/catalog/product/aldrich/471364?lang=en&region=US
ODE	1000 mL	35	$0.035/mL	http://www.sigmaaldrich.com/catalog/product/aldrich/o806?lang=en&region=US
$Zn(Ac)_2$	1000 g	77.2	$0.077/g	http://www.sigmaaldrich.com/catalog/product/sigald/z0625?lang=en&region=US
CdO	500 g	126.5	$0.25/g	http://www.sigmaaldrich.com/catalog/product/aldrich/244783?lang=en&region=US
$Mn(Ac)_2$	2000 g	129.5	$0.065/g	http://www.sigmaaldrich.com/catalog/product/aldrich/221007?lang=en&region=US
S	1000 g	34.9	$0.035/g	http://www.sigmaaldrich.com/catalog/product/sigald/13825?lang=en&region=US

Supplementary Table 4. Cost of chemicals for industrial-scale production

Chemical	Size	Price ($)	Unit-price	Source link
CuI	1000 g	50	$0.05/g	https://www.alibaba.com/product-detail/Copper-I-iodide_60514126494.html?spm=a2700.7724838.0.0.tvYoUk
$In(Ac)_3$	1000 g	400	$0.4/g	https://www.alibaba.com/product-detail/high-purity-99-9-INDIUM-ACETATE_60512060130.html?spm=a2700.7724838.0.0.sCGSIS
$Zn(St)_2$	1000 kg	1400	$0.0014/g	https://www.alibaba.com/product-detail/zinc-stearate-manufactures-china_60109497541.html?spm=a2700.7724838.0.0.2MZmaf
Se	1000 g	16	$0.016/g	https://www.alibaba.com/product-detail/High-Quality-Paint-Mitsui-Selenium_1536380133.html?spm=a2700.7724838.0.0.wc3rIa
OA	1120 L	1220	$0.0011/mL	https://www.alibaba.com/product-detail/hot-selling-best-price-of-industrial_60414494888.html?spm=a2700.7724838.0.0.ssFVTA

OAm	1230 L	4500	\$0.0036/mL	https://www.alibaba.com/product-detail/Oleylamine-112-90-3_1127391024.html?spm=a2700.7724838.0.0.Argrr6
DPP	934 mL	100	\$0.11/mL	https://www.alibaba.com/product-detail/DDP-Diphenylphosphine-CAS-829-85-6_1804413654.html?spm=a2700.7724838.0.0.sCQSGA
DDT	1180 mL	5	\$0.024/mL	https://www.alibaba.com/product-detail/High-purity-of-1-Dodecanethiol_60232347900.html?spm=a2700.7724838.0.0.Y2Vy9l
ODE	1270 mL	3	\$0.0024/mL	http://www.lookchem.com/product_1-Octadecene/2036426.html#formsend
$Zn(Ac)_2$	1000 kg	1200	\$0.0012/g	https://www.alibaba.com/product-detail/96-97-99-Zinc-acetate-for_60476709672.html?spm=a2700.7724838.0.0.o4qrTD&s=p
CdO	1000 kg	5500	\$0.0055/g	https://www.alibaba.com/product-detail/Brown-or-brownish-black-crystalline-powder_60279771032.html?spm=a2700.7724838.0.0.EjvJuQ

$Mn(Ac)_2$	1000 kg	1700	$0.0017/g	https://www.alibaba.com/product-detail/ Manganese-Acetate-99-_916973629.htm l?spm=a2700.7724838.0.0.prY19g
S	1000 kg	160	$0.00016/g	https://www.alibaba.com/product-detail/ granular-sulphur-99-9-_1148092469.htm l?spm=a2700.7724838.0.0.sFSGMF

Supplementary Table 5. Cost calculations for $CuInSe_2$/ZnS QDs

Chemicals	Lab-scale unit-price	Industrial unit-price	One-batch usage	Lab-scale cost	Industrial cost
CuI	$0.38/g	$0.05/g	0.11 g	$0.041	$0.0055
$In(Ac)_3$	$7.8/g	$0.4/g	0.17 g	$1.3	$0.068
$Zn(St)_2$	$0.036/g	$0.0014/g	6.3 g	$0.23	$0.0088
Se	$0.50/g	$0.016/g	0.095 g	$0.048	$0.0015
OA	$0.030/mL	$0.0011/mL	10 mL	$0.30	$0.011
OAm	$0.14/mL	$0.0036/mL	3 mL	$0.43	$0.011
DPP	$2.8/mL	$0.11/mL	0.3 mL	$0.84	$0.032
DDT	$0.024/mL	$0.024/mL	10 mL	$0.24	$0.042
ODE	$0.035/mL	$0.0024/mL	27.5 mL	$0.96	$0.065
Solvent cost for cleaning and processing[1]				$1.6	$0.10
Total cost of chemicals				$6.0	$0.34
Chemical yield of QDs				0.60 g	
Cost of chemicals per gram of QD				$10.0/g	$0.57/g

Non-material related expenses (equipment, labour, etc.)[2]	NA	\$0.016/g
Final price of QDs	> \$10.0/g	\$0.59/g

1. From ref. 2, based on a two-step purification procedure using hexane and ethanol.

2. Based on non-material-related expenses typical of Si-PV industry (see text for details).

Supplementary Table 6. Cost calculations for Mn^{2+}-doped $Cd_xZn_{1-x}S$/ZnS QDs

Chemicals	Lab-scale unit-price	Industrial unit-price	One-batch usage	Lab-scale cost	Industrial cost
$Zn(OAc)_2$	$0.077/g	$0.0012/g	1.4 g	$0.11	$0.0017
CdO	$0.25/g	$0.0055/g	0.064 g	$0.016	$0.00035
$Mn(OAc)_2$	$0.065/g	$0.0017/g	0.0085 g	$0.00055	$0.000014
S	$0.035/g	$0.00016/g	0.064 g	$0.0022	$0.000010
OA	$0.030/mL	$0.0011/mL	1 mL	$0.030	$0.0011
OAm	$0.14/mL	$0.0036/mL	5.4 mL	$0.77	$0.020
DDT	$0.024/mL	$0.024/mL	5 mL	$0.12	$0.021
ODE	$0.035/mL	$0.0024/mL	42 mL	$1.5	$0.099
Solvents for cleaning and processing				$1.6/g	$0.10/g
Total cost of chemicals				$4.1	$0.24
Chemical yield of QDs				0.75 g	
Total cost of chemicals per gram of QDs				$5.5/g	$0.32/g
Non-material related expenses (equipment, labour, etc.)				NA	$0.016/g

Final price of QDs	> $5.5/g	$0.34/g

Supplementary Table 7. Per-m^2 cost comparison between QD-LSCs and PVs

Component \ Device type	CISe-QD LSC	Mn –QD LSC	Si-PV
QDs[1]	$1.15	$0.38	NA
PVP	$0.24	$0.24	
Borosilicate substrate glass	$1	$1	
Other materials	$1		
Total cost	$5.01 (tandem LSC)		$100

1. The cost of QDs in a QD-LSC depends on the QD concentration. Costs listed here correspond to QD-LSCs in the tandem device studied in the present work.

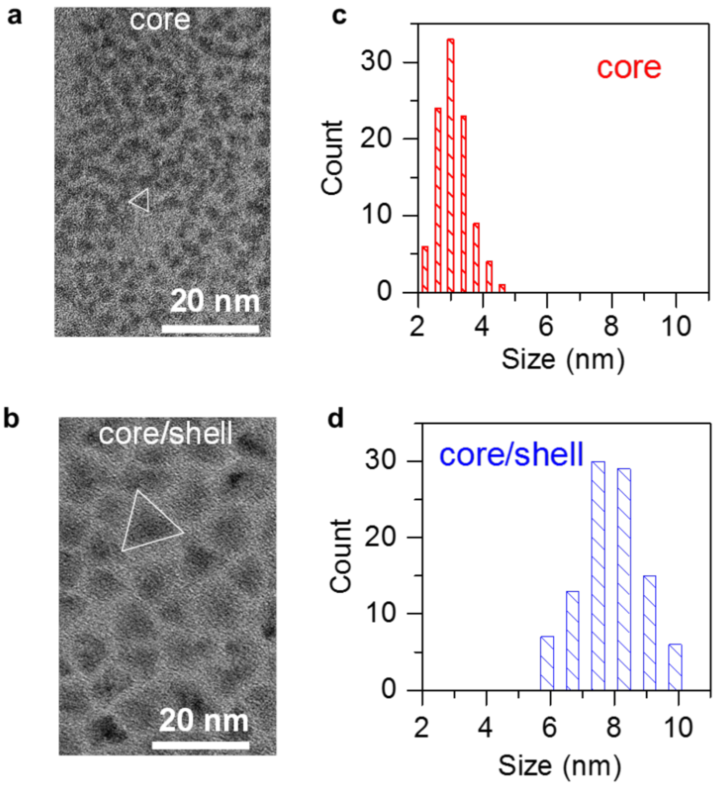

Supplementary Figure 1. TEM studies of CISe cores and CISe/ZnS core/shell QDs. a-b, TEM images of $CuInSe_2$ cores (a) and $CuInSe_2$/ZnS core/shell QDs (b). Both core and core/shell QDs have tetrahedral shapes. Their sizes are evaluated in terms of the length of a tetrahedral edge. **c-d,** Histograms of QD sizes for $CuInSe_2$ cores (c) and $CuInSe_2$ /ZnS core/shell QDs (d). The average sizes are 3.1±0.5 nm and 7.9±0.9 nm, respectively.

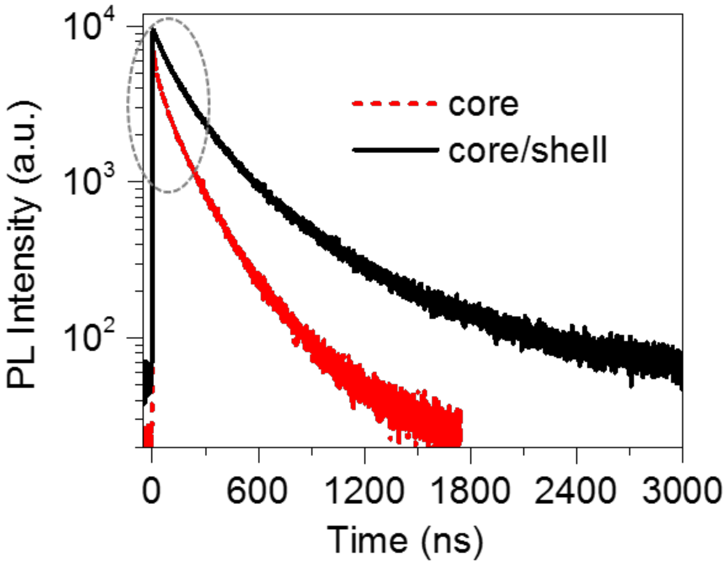

Supplementary Figure 2. PL dynamics of $CuInSe_2$ cores and $CuInSe_2$/ZnS core/shell QDs. The excitation source is a 405 nm laser diode with the pulse width of ~1 ns. The thick ZnS shell effectively passivates surface traps, which leads to slower PL dynamics (black) compared to core-only samples (red).

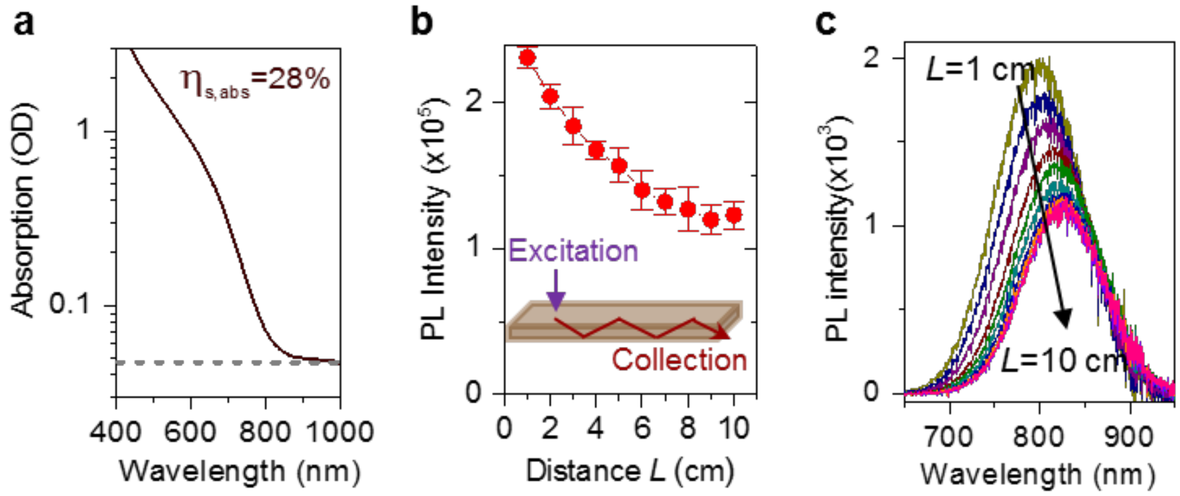

Supplementary Figure 3. Measurements of PL propagation losses in CISe-QD-based LSCs. a, An absorption spectrum of the LSC showing 28% absorptance ($\eta_{s,abs}$) for incident solar light. The LSC has very weak scattering, as indicated by the fact that the absorption spectrum shows no signatures of optical scattering in the intragap region but only exhibits a small constant offset arising from light reflections (~8% reflectivity). **b,** Spectrally integrated intensity of PL emerging from the LSC edge as a function of the distance (L) between the excitation spot and the collection edge (inset). **c,** The L- dependent PL spectra show the presence of weak re-absorption on the blue side of the spectra.

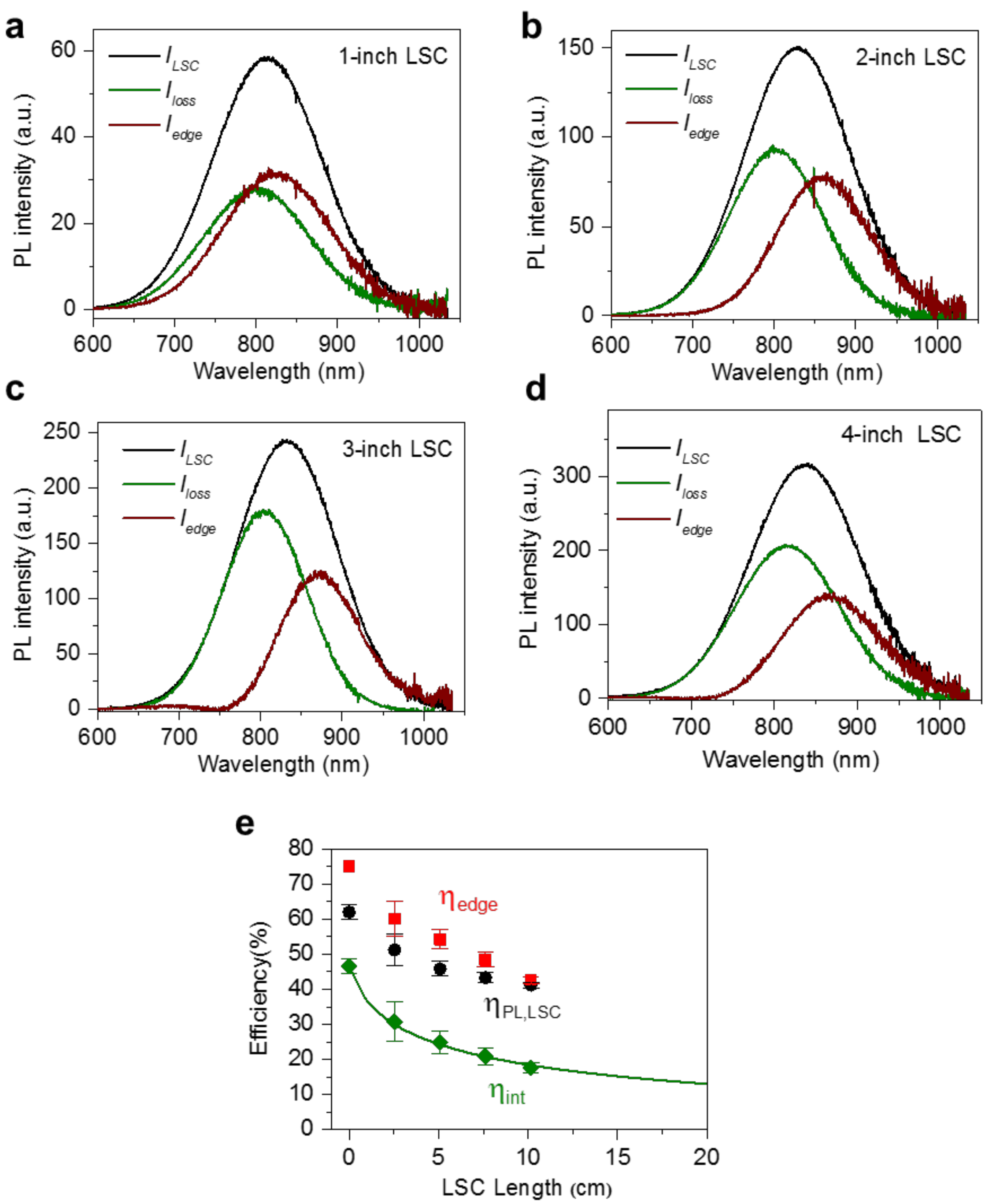

Supplementary Figure 4. Optical measurements of CISe-QD LSCs using an integrating-sphere. a-d, Emission spectra of LSCs for four different device sizes: 1×1 inch^2 (a), 2×2 inch^2 (b), 3×3 inch^2 (c), and 4×4 inch^2 (d). Black and green lines are the total LSC emission (I_{LSC}) and face-only emission (I_{loss}), respectively, obtained by measuring the emission spectra of the unmasked LSC and the LSC with the edges masked with a black tape.

The edge-emission spectrum (I_{edge}, brown) is obtained by subtracting the above two spectra. **e,** The PL QY of the LSC ($\eta_{\mathrm{PL,LSC,}}$; black circles), the edge-emission efficiency of the LSC (η_{edge}; red squares), and the internal quantum efficiency of the LSC (η_{int}; green diamonds) plotted as a function of LSC length. $\eta_{\mathrm{PL,LSC}}$ is obtained by dividing I_{LSC} by the absorbed flux of incident photons; η_{edge} is obtained from $\eta_{\mathrm{edge}}= I_{\mathrm{edge}}/I_{\mathrm{LSC}}$;[2,19] η_{int} is calculated from $\eta_{\mathrm{int}} = \eta_{\mathrm{PL,LSC}}\eta_{\mathrm{edge}}$.[2,19] The green solid line is a fit using eq. S4.

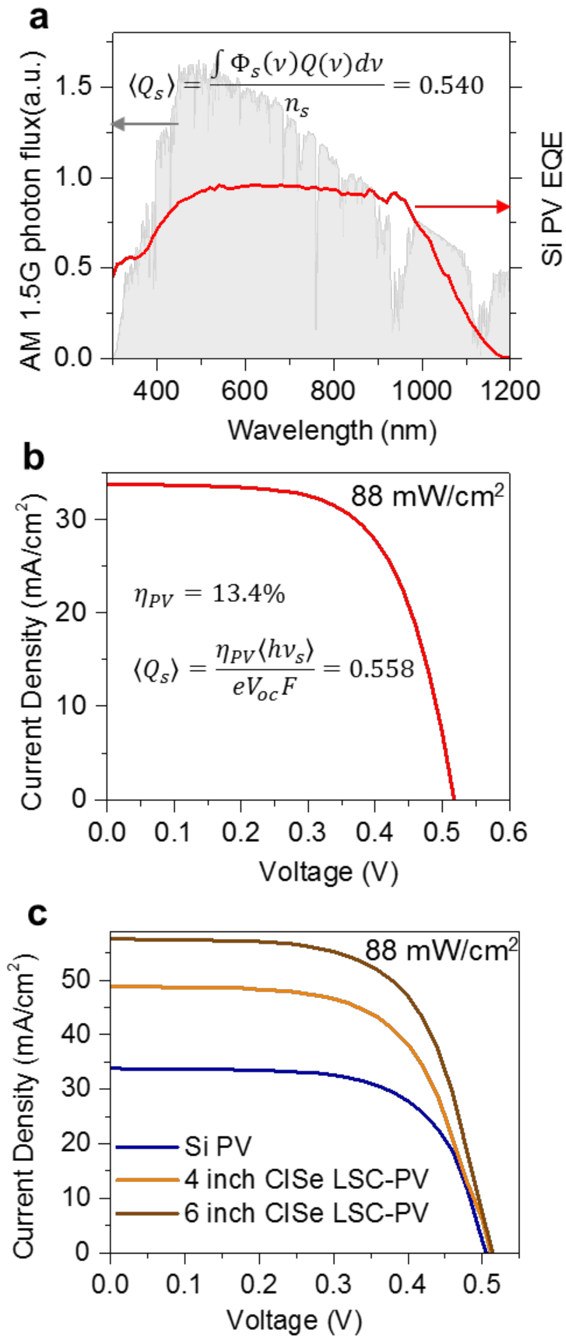

Supplementary Figure 5. Electro-optical measurements of CISe-QD LSCs. a, The EQE spectrum of the poly-crystalline PV cell (red) used in the present study is averaged over the solar photon flux spectrum (gray) to yield the averaged EQE (<Q_s>) of 0.540. In comparison, the EQEs averaged over the PL spectra of the CISe/ZnS and Mn^{2+}-doped QDs used in the present study are 0.92 and 0.95, respectively. **b,** From the *J-V* measurement (red) for the PV cell, the solar cell PCE (η_{PV}) is 13.4%. The averaged EQE ($<Q_s>$) calculated based on the measured short-circuit current is 0.558, which is in a good agreement with the value derived from the data in (a). **c,** The *J-V* curves of the polycrystalline-silicon PV (blue) and two coupled LSC-PV devices (light yellow is for the 4×4 inch^2 LSC; dark yellow is for the 6×6 inch^2 LSC) measured under natural outdoor illumination with the sunlight power of 88 mW/cm^2. The PCEs of LSC-PVs are: $\eta_{\text{LSC-PV}}$=0.90% for L = 10.16 cm, and $\eta_{\text{LSC-PV}}$=1.10% for L = 15.24 cm. The short circuit currents of the LSC-PV systems with L = 10.16 and 15.24 cm are, respectively, 1.44 and 1.71 times higher than J_{sc} of the standalone PV. Using the results of these measurements in eq. S6, we can derive η_{int} of the investigated LSCs (Fig. 2d).

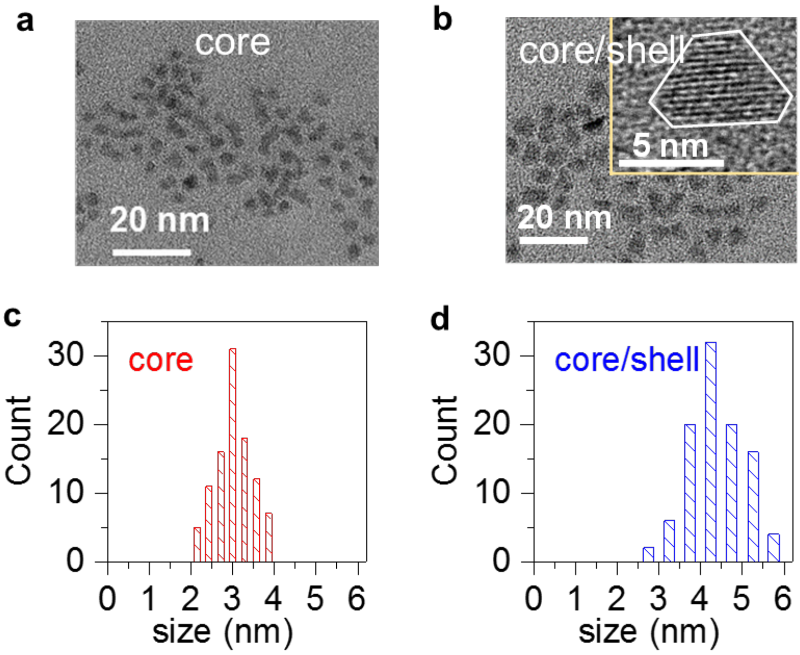

Supplementary Figure 6. TEM studies of Mn^{2+}:$Cd_xZn_{1-x}S$ cores and Mn^{2+}:$Cd_xZn_{1-x}S$/ZnS core/shell QDs. a-b, TEM images of the Mn^{2+}:$Cd_xZn_{1-x}S$ cores (a) and Mn^{2+}:$Cd_xZn_{1-x}S$/ZnS core/shell QDs (b). Inset in (b) is the high-resolution TEM image of an individual core/shell particle. **c-d,** Histograms of the sizes of the cores (c) and the core/shell QDs (d). The cores and core/shell QDs have average sizes of 3.0±0.4 nm and 4.4±0.6 nm, respectively.

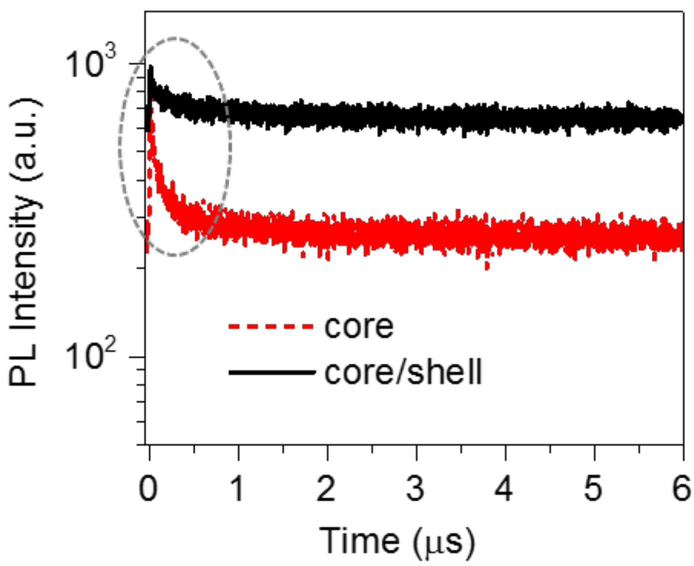

Supplementary Figure 7. **PL dynamics of Mn^{2+}:$Cd_xZn_{1-x}S$ cores and Mn^{2+}:$Cd_xZn_{1-x}S$/ZnS core/shell QDs.** The excitation source is a 405 nm laser diode with the pulse width of ~1 ns. A nearly complete elimination of the fast PL decay component upon a shelling procedure indicates successful passivation of surface defects by the ZnS shell.

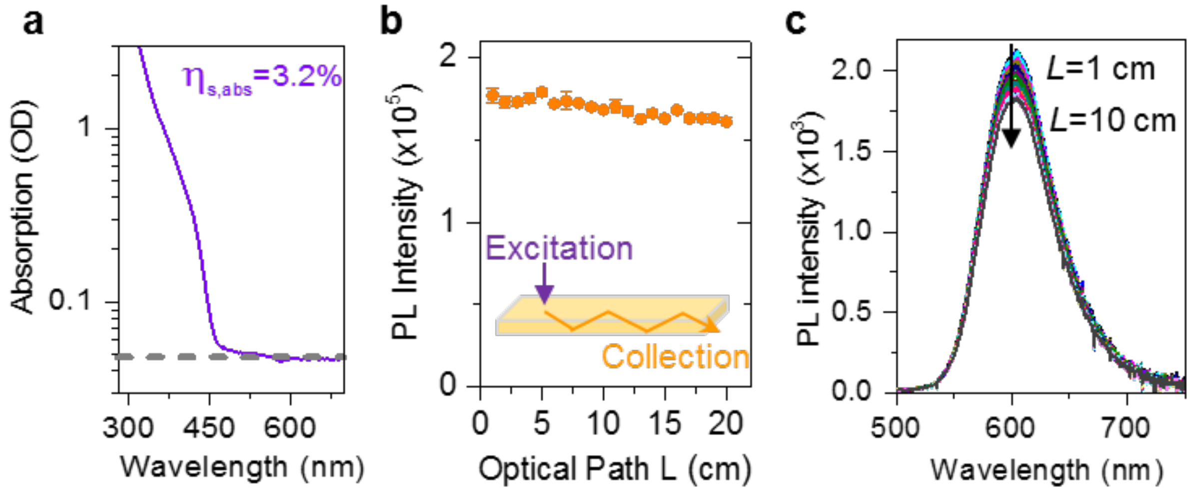

Supplementary Figure 8. Measurements of PL propagation losses in Mn-QD LSCs. a, An absorption spectrum of the LSC indicates sunlight absorptance ($\eta_{s,abs}$) of 3.2% and negligible scattering. **b,** Spectrally integrated intensity of PL from the LSC edge as a function of distance (*L*) between the excitation spot and the collection edge (inset). **c,** Edge emission spectra as a function of *L*. The PL profile is almost *L*-independent indicating virtually reabsorption-free propagation of reemitted light in the LSC waveguide. A weak spectrally uniform PL attenuation is due to weak scattering at optical imperfections within the LSC.

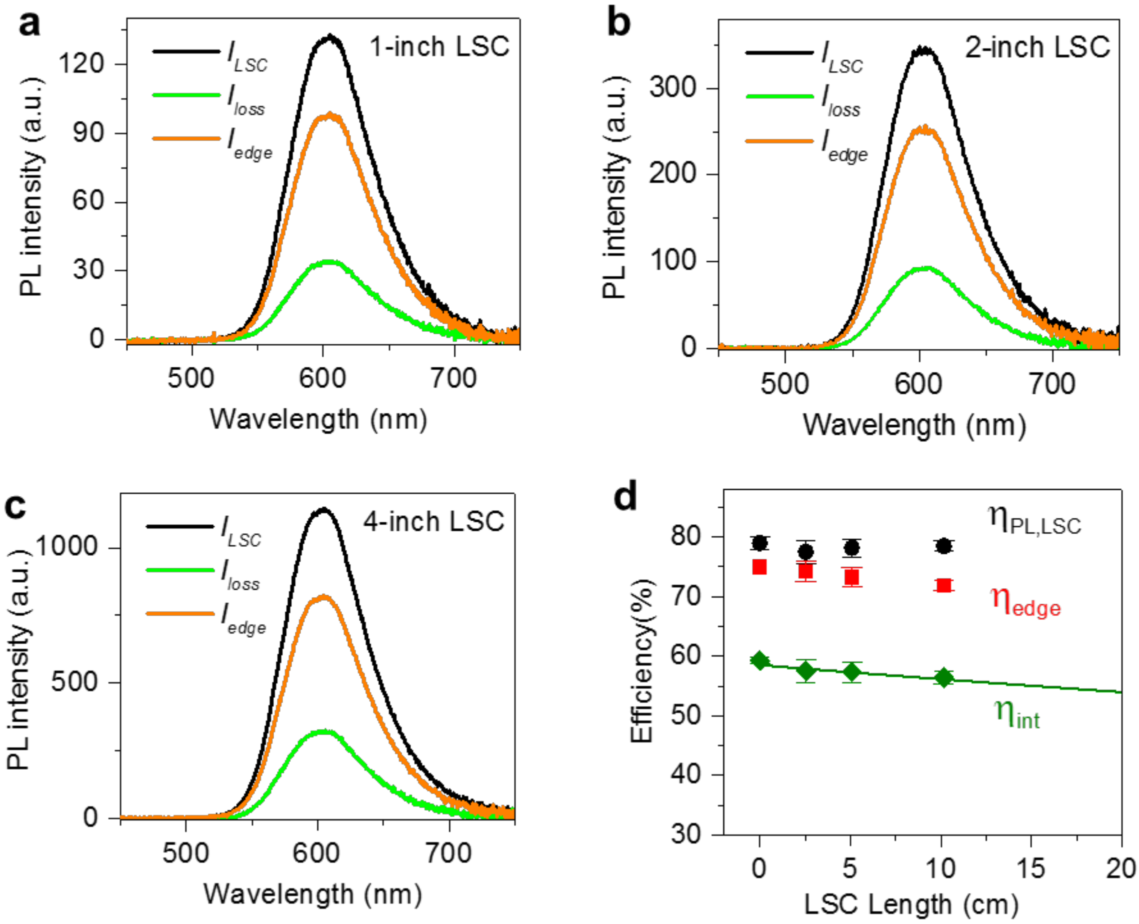

Supplementary Figure 9. Optical measurements of Mn-doped QD-based LSCs using an integrating-sphere. a-c, Same type of measurements and same notations as in Supplementary Fig. 4a-d for LSCs of three different sizes: 1×1 inch^2 (a), 2×2 inch^2 (b), and 4×4 inch^2 (c). **d,** Same as in Supplementary Fig. 4e but for Mn-doped QD LSCs. Due to "reabsorption-free" light propagation regime in LSCs based on Mn-doped QD, the drop in h_{int} with increasing L is almost exclusively due to scattering. Based on the conducted measurements, the scattering coefficient $s_2 = 0.012$ cm^{-1} (see Supplementary Note 1).

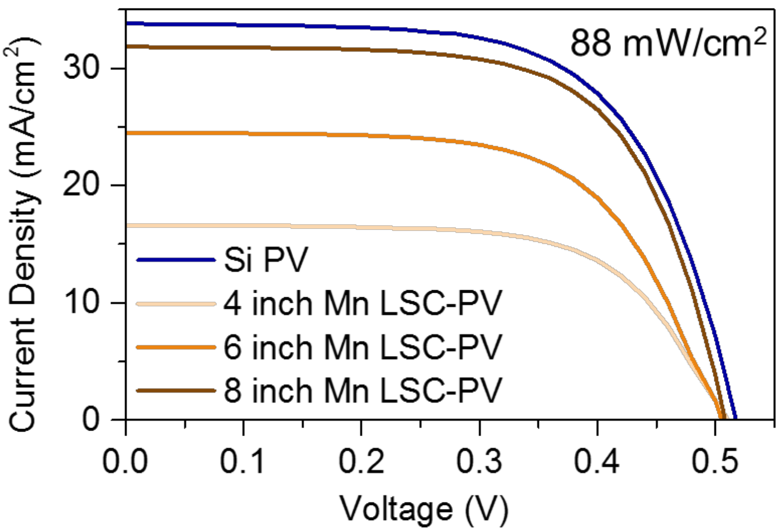

Supplementary Figure 10. Electro-optical measurements of Mn-doped QD-based LSCs. The *J-V* characteristics of a polycrystalline-silicon PV (blue) and three coupled LSC-PV devices (light yellow is for the 4×4 inch^2 LSC; medium yellow is for the 6×6 inch^2 LSC; dark yellow is for the 8×8 inch^2 LSC) measured under natural outdoor illumination with the sunlight power of 88 mW/cm^2. The PCEs of the LSC-PV systems are $\eta_{\text{LSC-PV}} = 0.39\%$ for $L = 10.16$ cm, $\eta_{\text{LSC-PV}} = 0.37\%$ for $L = 15.24$ cm, and $\eta_{\text{LSC-PV}} = 0.38\%$ for $L = 20.32$ cm. The short circuit currents of the LSC-PV systems with $L = 10.16$ cm, 15.24 cm, and 20.32 cm are, respectively, 0.49, 0.72, and 0.94 times that of the standalone PV. Using the results of these measurements in eq. S6, we can derive η_{int} of the investigated LSCs (Fig. 3c).

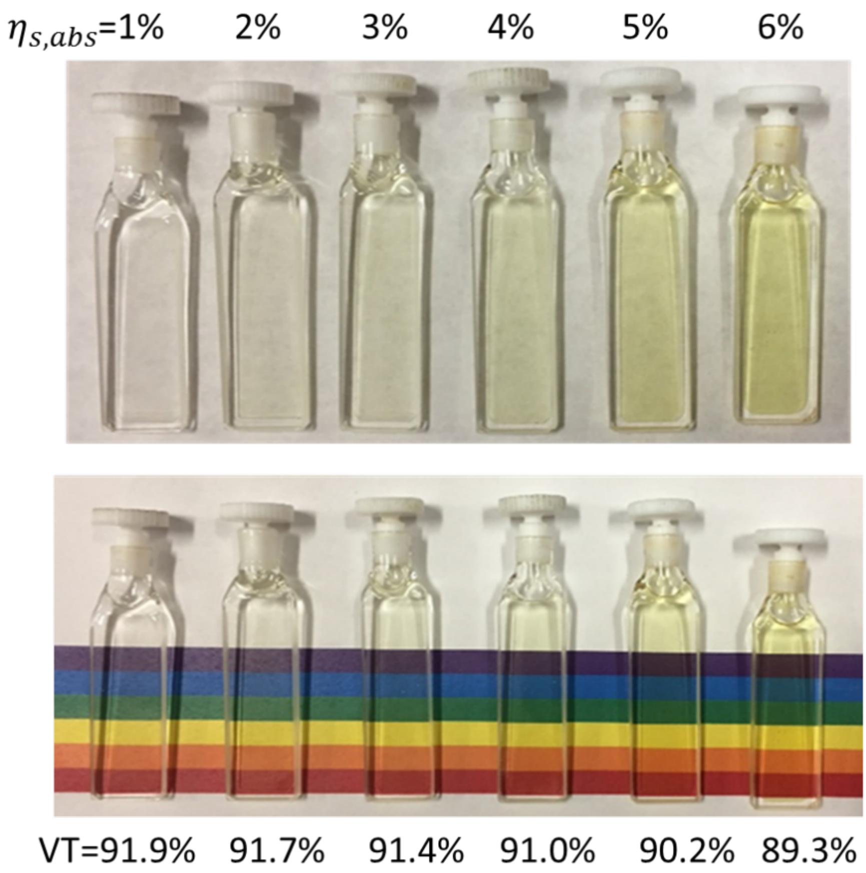

Supplementary Figure 11. Photograph of Mn^{2+}:$Cd_xZn_{1-x}S$/ZnS core/shell QDs with varied concentrations. Solar absorptances ($\eta_{s,abs}$) and visible transmittances (*VT*; calculated using eq. S7) of these samples are indicated in the figure.

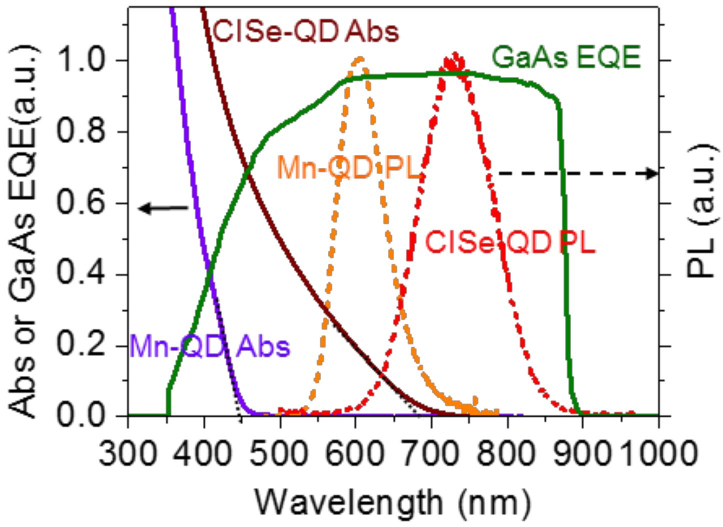

Supplementary Figure 12. Optical spectra of QDs and an EQE of GaAs solar cells used in the tandem device. The absorption (purple) and PL (orange; QY=78%) spectra of the Mn^{2+}-doped $Cd_xZn_{1-x}S$/ZnS core/shell QDs are exactly the same as those used in the single-layer LSC studies (Fig. 3). The $CuInSe_2$/ZnS core/shell QDs, used in the tandem are slightly different from those used in the single-layer device shown in Fig. 1b (bottom panel). Specifically, both the onset of strong absorption and the PL band for these dots are blue-shifted to, respectively, 680 nm (brown) and 750 nm (red); the PL QY is 72%. The green line is the EQE spectrum of the GaAs PV cells used in the LSC tandem devices. The EQE averaged over the solar photon flux spectrum ($<Q_s>$) is 0.401. In comparison, the EQEs averaged over the PL spectra of the CISe/ZnS and Mn^{2+}-doped QDs used in the tandem are 0.852 and 0.946, respectively; the latter values correspond to the "spectral re-shaping" factors (q) of 2.12 (CISe-based QDs) and 2.36 (Mn^{2+}-doped QDs).

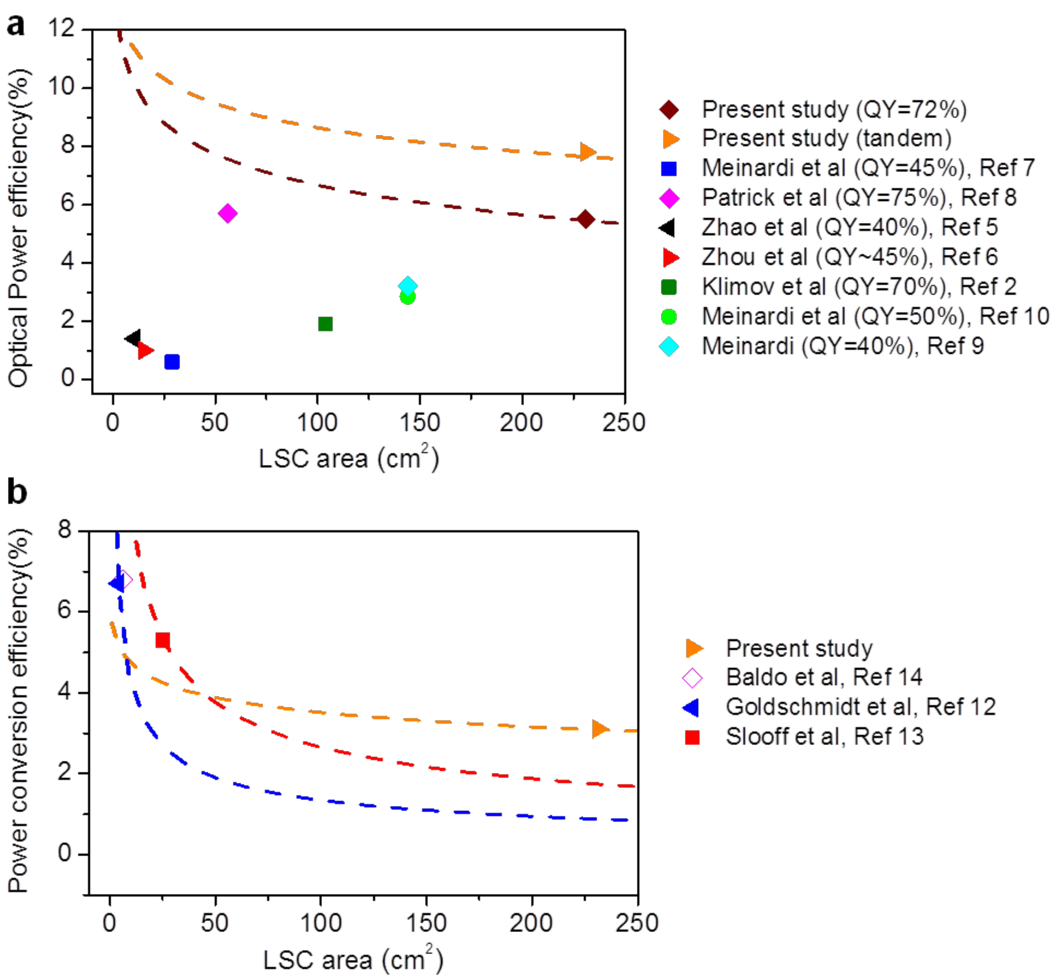

Supplementary Figure 13. Comparison of present devices with literature QD- and dye-molecule-based LSCs. a, A plot of the optical power efficiency ($\eta_{s,p}$; coloured symbols) as a function of the LSC area for the QD-LSCs listed in Supplementary Table 1. The dashed lines are the extrapolated $\eta_{s,p}$ data obtained using the size-dependent LSC efficiencies reported in Figure 2c,d of the main text. Both the single-layer CISe-QD LSCs and tandem devices from the present work are superior to QD-LSCs reported in the literature for all size regimes. **b,** A plot of the power conversion efficiency (PCE; coloured symbols) as a function of the LSC area for the dye-based LSCs listed in Supplementary Table 2. The value from ref. 14 (shown with an open symbol) is not a directly-measured result but an estimation based on single-wavelength, point-by-point excitation measurements. Other data points (solid symbols) are obtained from direct measurements. The dashed lines are the extrapolated efficiency curves. For ref. 12 and ref. 13, the extrapolation is based on the fact that the efficiency of a conventional LSC scales inversely with the LSC size (L) according to eq. S2. For our present tandem devices, however, the use of a zero-reabsorption top layer slows the efficiency drop with increasing LSC size, especially at larger sizes ($L^2 > 50$ cm^2); the extrapolation uses the size-dependent LSC efficiencies reported in Figure 2c,d of the main text. Although for smaller areas (<50 cm^2), PCEs of our devices are slightly lower than the best literature values for dye-based LSCs, the QD tandems are expected to significantly outperform dye-based LSCs in the case of larger area devices.

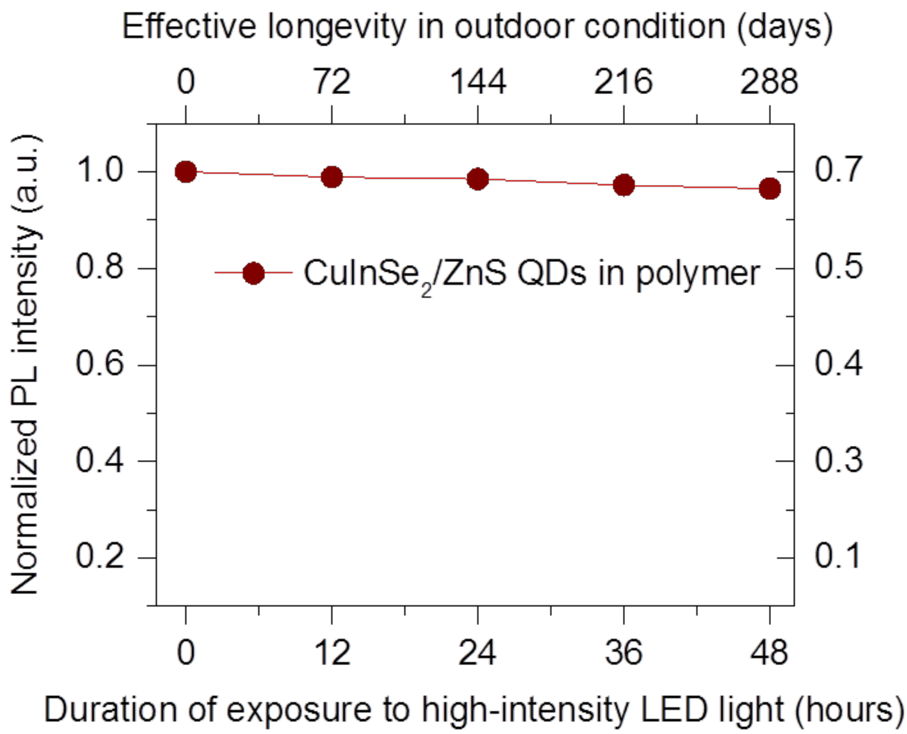

Supplementary Figure 14. Accelerated stability test on CISe QD/PVP composites. The film was fabricated by drop-casting the QD/PVP composite onto a coversilp and then loaded into a customized airtight cuvette under N_2 atmosphere in a glove box. The excitation source was a 462 nm LED with intensity 1.57 W/cm^2, which corresponded to the acceleration factor of 56 (see Methods).

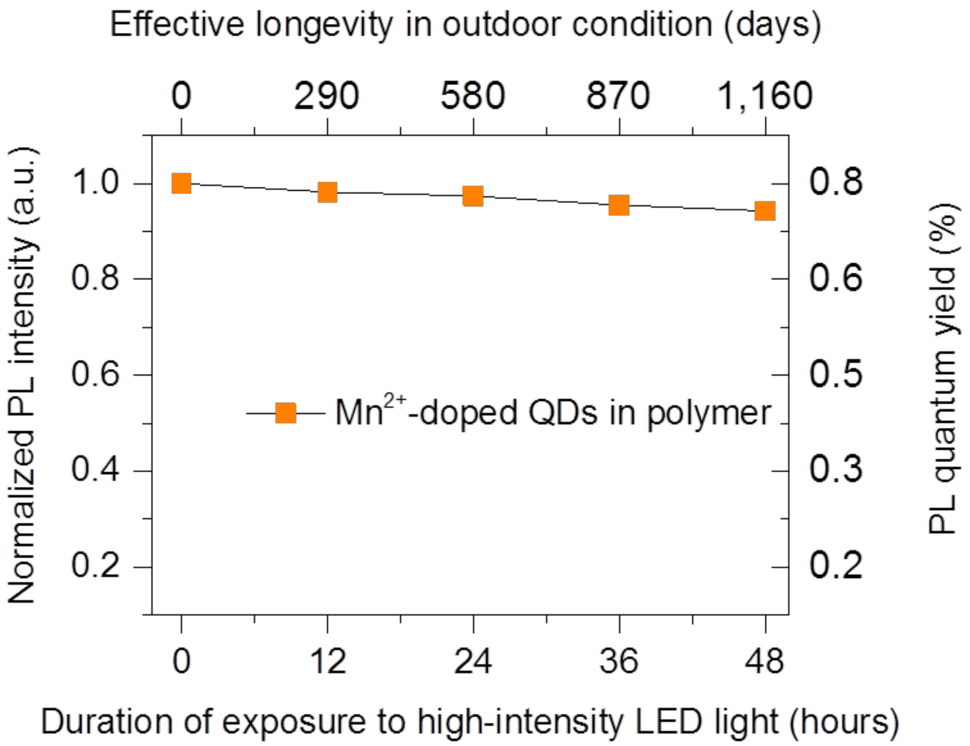

Supplementary Figure 15. Accelerated stability test on Mn^{2+}-doped QD/PVP composites. The film was fabricated by drop-casting the QD/PVP composite onto a coversilp and then loaded into a customized airtight cuvette under N_2 atmosphere in a glove box. The excitation source was a 405 nm LED with intensity 0.75 W/cm^2, which corresponded to the acceleration factor of 230.

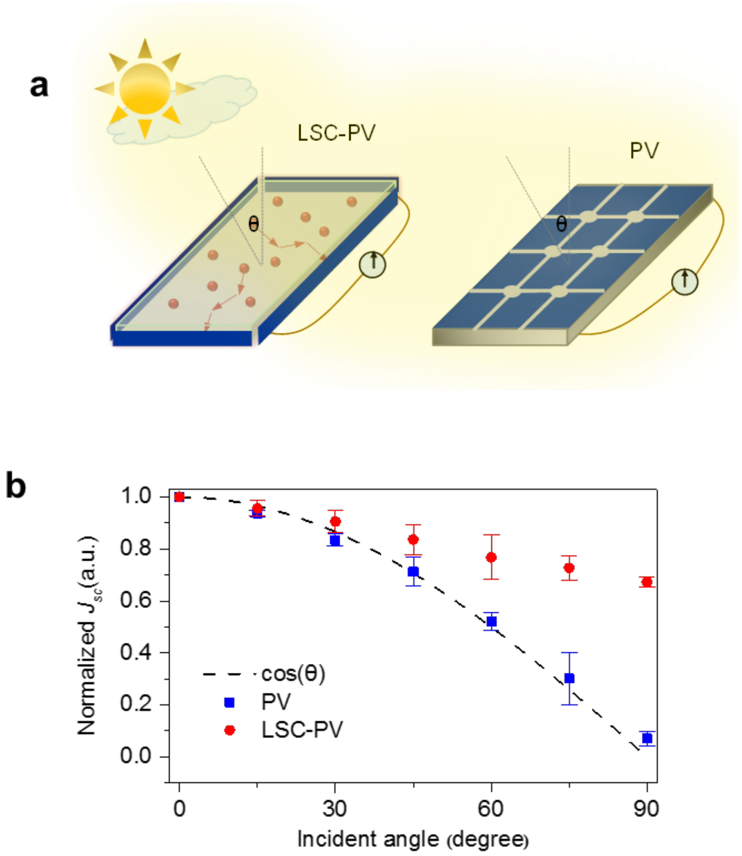

Supplementary Figure 16. The incident angle dependence of the short-circuit current of a standalone PV and a coupled LSC-PV device. a, Schematic representations of a coupled LSC-PV device (left) and a standalone PV device (right) with the same effective light-harvesting area. **b,** The measured dependence of normalized short-circuit currents (J_{sc}) on the incident angle (θ) of solar radiation for a PV cell (solid blue square) and the same cell coupled to a QD LSC (solid red circle). The black dashed line is an ideal cos(θ) dependence. The J_{sc} of an LSC-PV device maintains ~68% of its peak value when rotated to θ=90°, while the J_{sc} of the PV drops to ~6% of its peak value for the same angle.

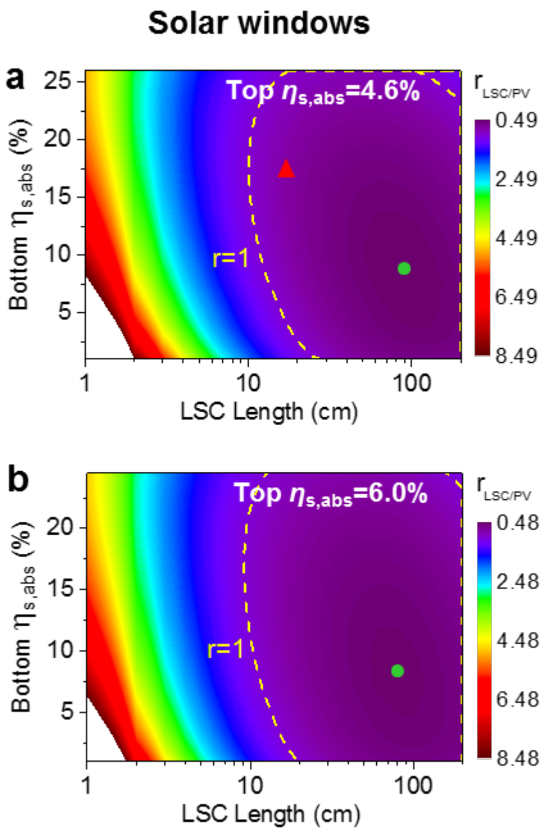

Supplementary Figure 17. The LSC cost-efficiency factor ($r_{LSC/PV}$) for building integrated devices when the cost of glass is excluded from price estimations. a, The solar absorptance of the top layer is fixed at 4.6%, as in the tandem LSC reported in the main text. The $r_{LSC/PV}$ is plotted as a function of the LSC size and the absorptance of the bottom layer. The yellow dashed line corresponds to $r_{LSC/PV}$=1; it circles the region where an LSC-PV device is more cost-effective than a standalone PV. The global minimum in this plot (green circle) corresponds to $r_{LSC/PV}$ =0.49, indicating a cost saving of 51%. The red triangle represents the tandem LSC shown in Fig. 4a, for which $r_{LSC/PV}$ =0.77 (23% cost saving). **b,** The same calculations performed for tandem LSCs with the absorptance of the top layer of 6.0%, which corresponds to the maximum value achievable with our Mn-doped QDs. The cost saving in this case is increased to 52%.

Supplementary References

1. Klimov, V.I., Baker, T.A., Lim, J., Velizhanin, K.A. & McDaniel, H. Quality factor of luminescent solar concentrators and practical concentration limits attainable with semiconductor quantum dots. *ACS Photonics* **3**, 1138-1148 (2016).
2. Li, H., Wu, K., Lim, J., Song, H.-J. & Klimov, V.I. Doctor-blade deposition of quantum dots onto standard window glass for low-loss large-area luminescent solar concentrators. *Nat. Energy* **1**, 16157 (2016).
3. Lunt, R.R. Theoretical limits for visibly transparent photovoltaics. *Appl. Phys. Lett.* **101**, 043902 (2012).
4. Tuchinda, C., Srivannaboon, S. & Lim, H.W. Photoprotection by window glass, automobile glass, and sunglasses. *J. Am. Acad. Dermatol.* **54**, 845-854 (2006).
5. Zhao, H. *et al.* Absorption enhancement in "giant" core/alloyed-shell quantum dots for luminescent solar concentrator. *Small* **12**, 5354-5365 (2016).
6. Zhou, Y. *et al.* Nearinfrared, highly efficient luminescent solar concentrators. *Adv. Energ. Mater.* **6**, 1501913 (2016).
7. Meinardi, F. *et al.* Large-area luminescent solar concentrators based on 'Stokes-shift-engineered' nanocrystals in a mass-polymerized PMMA matrix. *Nat. Photon.* **8**, 392-399 (2014).
8. Sumner, R. *et al.* Analysis of optical losses in high-efficiency $CuInS_2$-based nanocrystal luminescent solar concentrators: balancing absorption versus scattering. *J. Phys. Chem. C* **121**, 3252-3260 (2017).
9. Meinardi, F. *et al.* Highly efficient large-area colourless luminescent solar concentrators using heavy-metal-free colloidal quantum dots. *Nat. Nanotechnol.* **10**, 878-885 (2015).
10. Meinardi, F. *et al.* Highly efficient luminescent solar concentrators based on earth-abundant indirect-bandgap silicon quantum dots. *Nat. Photon.* **11**, 177-185 (2017).
11. Bomm, J. *et al.* Fabrication and full characterization of state-of-the-art quantum dot luminescent solar concentrators. *Sol. Energ. Mat. Sol. Cells* **95**, 2087-2094 (2011).
12. Goldschmidt, J.C. *et al.* Increasing the efficiency of fluorescent concentrator systems. *Sol. Energ. Mat. Sol. Cells* **93**, 176-182 (2009).
13. Slooff, L.H. *et al.* A luminescent solar concentrator with 7.1% power conversion efficiency. *Phys. Status Solidi Rapid Res. Lett.* **2**, 257-259 (2008).
14. Currie, M.J., Mapel, J.K., Heidel, T.D., Goffri, S. & Baldo, M.A. High-efficiency organic solar concentrators for photovoltaics. *Science* **321**, 226-228 (2008).
15. Wittwer, V., Stahl, W. & Goetzberger, A. Fluorescent planar concentrators. *Sol. Energ. Mater.* **11**, 187-197 (1984).
16. Zhao, Y., Meek, G.A., Levine, B.G. & Lunt, R.R. Near-infrared harvesting transparent luminescent solar concentrators. *Adv. Opt. Mater.* **2**, 606-611 (2014).
17. Zhao, Y. & Lunt, R.R. Transparent luminescent solar concentrators for large-area solar windows enabled by massive Stokes-shift nanocluster phosphors. *Adv. Energ. Mater.* **3**, 1143-1148 (2013).

18. Lewis, N.S. Research opportunities to advance solar energy utilization. *Science* **351**, 10.1126/science.aad1920 (2016).
19. Coropceanu, I. & Bawendi, M.G. Core/shell quantum dot based luminescent solar concentrators with reduced reabsorption and enhanced efficiency. *Nano Lett.* **14**, 4097-4101 (2014).